LEX LOCALIS-JOURNAL OF LOCAL SELF-GOVERNMENT
ISSN:1581-5374 E-ISSN:1855-363X
VOL. 24, NO. 3 (2026)

DEEP NEURAL NETWORK-CONTROLLED ISOLATED THREE-PORT INTERLEAVED FLYBACK BOOST CONVERTER FOR SMART LOCAL ENERGY GOVERNANCE IN GRID-CONNECTED PHOTOVOLTAIC SYSTEMS

[1*]R. Sivakumar, [2]A. Manikandan, [3]S.Saranya Devi, [4] Kadirvel G

[1]Professor, [2,3,4] Assistant Professor,
[1,4] Department of CSE(IoT) ,[2,3] Department of AI & DS
[1,2,3] Paavai Engineering College, Namakkal, Tamil Nadu, India
[4]The Kavery Engineering College, Salem, Tamil Nadu, India
Corresponding Author:1*siva89grasc@gmail.com
Received: 19/02/2026; Accepted: 30/06/2026

Abstract: The energy management architectures for grid-connected PV energy systems must be high-efficiency, multi-port power conversion topologies that can manage energy simultaneously from PV energy resources, battery storage and the utility grid; but conventional isolated PV power conversion suffers from poor dynamic response, suboptimal switching coordination, and limited adaptability to variable irradiance and load conditions. The conventional control methods such as LSTM networks, GA-tuned controllers and traditional ML classifiers suffer from various drawbacks, including slow convergence, high computational requirements, and lack of transferability from nonlinear operation of three-port topologies. For isolated three-port interleaved flyback boost converter (ITIFBC), this work proposes a novel DNN controlled ITIFBC based on a multilayer perceptron (MLP), which is trained using 12,000 pre-processed operating samples with feature normalization, SMOTE oversampling and wrapper-based RFE. The DNN, optimized by Adam, controls the real-time duty-cycle modulation and interleaving phase-shifting of the three ports, maximizing power transfer efficiency on all three ports concurrently. Evaluated using MAE, RMSE, η, THD, VRA, and PF, the proposed system achieves η = 97.4%, THD = 1.37% (−62.3% over PI), RMSE = 0.0031, R^2 = 0.9981, dynamic response improvement of 41.7% over LSTM, VRA = 99.2%, and PF = 0.991.Overall, DNN-driven control holds significant promise for improving the reliability, scalability, and energy output of PV systems in grid-connected applications and smart microgrids, making it a valuable solution for future renewable energy integration and smart grid applications.

Keywords: Deep Neural Network (DNN) Control; Isolated Three-Port Flyback Boost Converter; Grid-Connected Photovoltaic Energy Systems; Interleaved Power Conversion Architecture; Smart Microgrid Energy Management; Adaptive Moment Estimation Optimization; Total Harmonic Distortion Suppression, Intelligent Energy Management; Local Energy Governance; Smart Municipal Energy Systems.

1.Introduction

In recent years, the world has seen a rapid shift towards decarbonized energy infrastructures, putting PV systems at the forefront of modern energy generation, and the number of grid-connected deployments has increased at a scale never before seen [1]. To meet these requirements, high performance power electronic converters need to control energy flow in both directions, provide galvanic isolation and provide high conversion efficiency in very demanding environmental and load conditions [2]. The Isolated Three-Port Interleaved Flyback Boost Converter (ITIFBC) has been a subject of great research interest due to its small magnetic structure, built-in voltage step up feature and capacity to connect various energy sources [3]. The interleaved configuration eliminates the input current ripple and reduces switching loss, which is attractive for the high-density PV micro-inverter systems [4]. However, it is obvious that the full performance potential of ITIFBC topologies can only be achieved with topologies that have advanced control methods that are able to dynamically adjust duty-cycle modulation and phase-shift coordination across all three ports in real-time, which conventional PI and PID regulators are inadequate to achieve [5].

The previous research literature has investigated LSTM networks [6], controllers optimized using the GA [7], traditional ML classifiers [8] and MPC frameworks [9] with prohibitive limitations such as inference latency, optimization without online experimentation, limited generalization capabilities, plant-model dependent controllers, and lack of representational depth for simultaneous multi-port control. These are the key factors that inspire the implementation of this paper, which suggests DNN-controlled ITIFBC framework.

1.1 Local Governance Perspective

The rapid transition toward renewable energy is not only a technological challenge but also a governance responsibility for local authorities. Municipal governments are increasingly responsible for planning distributed renewable energy infrastructure, improving energy resilience, reducing operational costs of public facilities, and supporting community-level sustainability initiatives. Intelligent photovoltaic energy systems equipped with adaptive control mechanisms can assist local administrations in maintaining stable electricity supply for public buildings, water treatment facilities, healthcare centres, educational institutions, and municipal microgrids. The proposed DNN-controlled ITIFBC contributes to these objectives by enabling efficient coordination between photovoltaic generation, battery storage, and grid interaction. Such intelligent energy management supports local governments in reducing transmission losses, improving renewable energy utilization, enhancing energy security, and facilitating the implementation of smart city initiatives. Consequently, the proposed framework extends beyond converter optimization by providing a technological foundation for sustainable local energy governance and resilient municipal power infrastructure.

In the paper, the works related to the proposed methodology are reviewed in Section 2, the proposed methodology is presented with full mathematical formulation in Section 3, quantitative result with embedded graphical analysis and discussion are summarized in Section 4, while future directions are concluded in Section 5.

2. Related Works

The existing control methods for grid connected photovoltaic (PV) converter system can be summarized into four general methodological categories: traditional linear and passive circuit-based controllers, metaheuristic optimized and neuro-fuzzy hybrid controllers, model-based predictive control (MPC) methods and data-driven intelligent methods. Forming a critical and comprehensive overview of representative pieces in each category, one can identify a systematic increase in performance trade-offs that together reveal an enduring series of problems that are not yet solved, whose solutions motivate the design goals of the proposed DNN-ITIFBC framework.

Sadhasivam and Sathyamoorthy [11] assessed the performance of an enhanced fuzzy logic controller (E-FLC) for differential power processing converter (DPPC) of solar PV system and found that the transient response is improved which can be measured as compared to traditional PI control. The modifications of passive circuit flyback converter using reverse-recovery suppression technologies [12] were successfully reported with efficiency improvement in single-phase continuous conduction mode, but both of them are open-loop in nature and do not offer any solution for adaptive duty cycle, state of charge awareness, and multi-port power flow coordination. It is, therefore, unsuitable to use passive-only topologies for the proposed ITIFBC architecture, which requires simultaneous three-port energy management. Both of these works exhibit a common drawback of the established paradigm: the converter operates well in a narrow range of well-defined operating points (steady-state performance), but when operating point moves away from its design value, the converter performance degrades — precisely the conditions that prevail in the real field deployment of PV.

Bhavani et al. [13] proposed a seven-level PV-wind converter for which an ANFIS-based controller was augmented with cuckoo search (CS) and grey wolf optimizer (GWO) algorithm to obtain better steady-state efficiency. The iterative population based optimization loops of GWO, however, have a computational burden that grows unfavorably with the number of decision variables and cannot be done in real time switching period without major pre-computation in the offline stage, which makes the method impractical for converters that need cycle-by-cycle adaptive control. Bhayo et al. [15] proposed a neural-fuzzy sliding mode controller for hybrid AC/DC microgrids with PV, wind, and battery systems and tested in simulated environments. However, the fixed-membership fuzzy rules are hard-coded in the controller and this generalization failure is directly present as high THD and voltage regulation error in the unknown operating regime during the load change. The two major drawbacks of the collective operation of the metaheuristic and the ANFIS in this category are offline (heuristic) hyperparameter tuning, which cannot cope with the real-time converter dynamics, and no adaptive selection of features in the high dimensional, nonlinear operating space of the three-port isolated converter topologies.

Alharbi et al. [16] gave a thorough survey of finite-control-set MPC (FCS-MPC) strategies for PV inverter applications in grid connected mode, explicitly pointing out two unresolved structural limitations: (1) an inability to guarantee fixed switching frequency, so that variable harmonic spectra are generated that make passive filter design difficult; and (2) the rapidly increasing online computation cost as the prediction horizon and dimension of the system state increase. In [17] Ahmed et al. developed a reduced sensor finite-set MPC framework using an extended Kalman filter (EKF) to obtain a fast transient response as compared to the conventional PI for MPPT applications. However, this approach is highly sensitive to a good small-signal plant model, and any drift of the converter parameters from their nominal values — whether it is caused by the components aging, thermal drift of the components or manufacturing tolerance — directly impacts the accuracy of the prediction and hence the closed-loop control performance, which is a robustness issue that can be very important in field converters that have been deployed for many years. Dekhane [18] presented an advanced FCS-MPC strategy for PV inverters with modifications of the cost function to ensure compliance during a voltage sag in the grid, resulting in better fault ride through performance. But the weights of the cost function, which balance the different control goals, e.g., minimizing harmonics versus minimizing switching frequency, had to be tuned by the experts and there was no provision for real-time adaptive tuning of these weights. The lack of such adaptability is a serious shortcoming: when operating conditions of the system change drastically, the controller needs to be redesigned, which not only requires engineering effort, but also poses an operational risk if the system is autonomous and smart microgrids are to be deployed.

De Silva et al. [19] proposed an adaptive meta-learning DDPG (AM-DDPG) reinforcement learning controller for voltage regulation of the three-leg interleaved boost converter in a PV system, which is impractical for deployment. In addition, battery state-of-charge was not used as a control input, limiting the use of the framework to the non-simultaneous topologies where PV and battery port control is the primary control objective.

Most critically, this approach was not applied to three-port isolated architectures, and the lack of THD evaluation metrics leaves unanswered the question of whether such efficiency gains are associated with affordable levels of harmonic injection to the grid interface, where the requirement for compliance is part of the IEEE 519 standard. In their work, Shahria et al. [21] compared the proximal policy optimization (PPO) approach of RL with the PI controller with shallow ANN controller for voltage regulation of a DC-DC boost converter and verified the superiority of RL in terms of step response settling time. Sarvi and Mohammad [22] critically reviewed the existing literature on DC-DC converter control and topologies for DC microgrid applications in a comprehensive manner, finding that none of the existing control paradigms in the literature fully meet the four concurrent requirements of galvanic isolation, simultaneous multi-port power management, real-time adaptive control within switching-period constraints, and minimal harmonic injection at the grid interface which in turn provides a clear delineation of the research gap that motivated the proposed DNN-ITIFBC framework. table 1 shows the Comparative summary of related control methods for grid-connected PV converter systems

Table 1. Comparative summary of related control methods for grid-connected PV converter systems.

Ref.	Method	Topology	Eff.%	THD%	Ports	Iso.	Key Limitation	Year
[11]	Enhanced FLC	DPP Converter	~94.5	N/R	2	No	Manual rule-base	2024
[12]	Passive+PI	Flyback CCM	~95.2	N/R	1	Yes	No adaptive ctrl	2024
[13]	ANFIS-GWO	7-Level Conv.	~95.8	~3.1	2	No	High computation	2024
[14]	ANN+Fuzzy	Boost+Inv.	~96.1	~2.8	2	No	Shallow ANN	2025
[15]	Neural-SMC	AC/DC MG	~95.4	~3.5	3	No	Fixed rules	2025
[16]	FCS-MPC Rev.	PV Inverter	~96.0	~2.5	2	No	High compute	2025
[17]	FS-MPC+EKF	Boost+PV	~95.7	~2.9	2	No	Model-dependent	2025
[18]	Adv.FCS-MPC	PV Inverter	~96.3	~2.3	2	No	Manual weights	2026
[19]	AM-DDPG RL	Intlvd.Boost	~96.5	N/R	2	No	Training instab.	2025
[20]	DRL+BFO	Intlvd.Boost	~97.0	N/R	2	No	2-port only	2025
[21]	PPO-RL	DC-DC Boost	~95.9	N/R	1	No	Sample-inefficient	2024

N/R = Not Reported. Eff. = Conversion Efficiency (%). THD = Total Harmonic Distortion. Iso. = Galvanic Isolation.

Identified Research Gaps, the reviewed literature in this survey shows that there are four recurring and interrelated gaps in the existing literature which are not addressed together in any existing work. First, all of the surveyed approaches do not have an adaptive, data-driven method that encodes the nonlinear relationships among the nine heterogeneous operating state variables at three physically separate ports in a single real-time inference cycle. Second, all optimization-based and model-driven approaches involve off-line hyper-parameter tuning, prior to execution, which is independent from the actual converter dynamics, making autonomous adaptation to parameter drift and/or operating conditions impossible. Third, the LSTM and shallow ANN architectures suffer from poor long term prediction stability when there are irradiance transients, because of sequential dependence and lack of representational depth, respectively. Fourth, none of the reviewed methods simultaneously optimizes duty-cycle modulation and interleaving phase-shift for the simultaneous power balancing in a galvanically isolated topology. The proposed DNN-ITIFBC is the first model that combines SMOTE-augmented multilayer perceptron-based adaptive feature extraction and Adam-optimized real-time co-regulation of d_1, d_2 and φ in a single, deployable framework, managing all four gaps.

3. Proposed Methodology

This section includes the complete design of Deep Neural Network controlled Isolated Three-Port Interleaved Flyback Boost Converter (DNN-ITIFBC) and its mathematical formulation and operational steps of the proposed PV energy system for high efficiency grid connected energy systems. The proposed scheme comprehensively tackles the four research gaps discussed in Section 2 by following a single pipeline of five stages: multi-sensor data acquisition, Feature-aware preprocessing, MLP inference, Dual-channel control signal generation, and Closed-loop adaptive feedback. Next, each stage is explained in detail with the relevant mathematical models, the full circuit schematic, the system block diagram and the complete algorithmic flow for each step, making the entire circuit schematic, block diagram and algorithm flow the novelty and implementational completeness of the proposed architecture.

3.1 Overall System Architecture

This proposed framework combines a Deep Neural Network (DNN) controller with an Isolated Three-Port Interleaved Flyback Boost Converter (ITIFBC) to enable the simultaneous real-time control of power at all three ports (PV source, battery storage, and grid port). The five-stage pipeline is shown below in Figure 1, which includes multi-sensor data acquisition, feature-aware preprocessing, DNN inference, generation of the dual-channel control signal, and closed-loop feedback. Design real-time system block diagram. The five stages are: from the three source nodes (PV array, battery bank, utility grid); to the data acquisition block (sensors, ADC, 12,000 sample dataset); to the preprocessing pipeline (min-max normalisation, SMOTE oversampling, RFE 9 feature selection); to the DNN controller block (input layer 9 nodes, hidden layers 128–64–32 ReLU, output layer d_1 d_2 φ, Adam optimiser, MSE loss); to the dual control signal generators (PWM duty-cycle generator d_1 d_2 with 180° interleaving, and phase-shift controller φ for three-port power routing); to the ITIFBC power stage (HF transformer, active clamp, voltage multiplier, f_{sw} = 50 kHz); to the three port output terminals (Port 1 PV, Port 2 Battery, Port 3 Grid); to the output measurement and feedback block ($V_{out}, THD, SOC, error\ e = V_{ref} - V_{out}$); to the dashed closed-loop feedback arc, which returns the measured error to the DNN loss update path. All bus tap and bus merge points are marked with the junction dots (●). The performance metrics panel (on the right) displays 7 real-time quality metrics in bar graphs

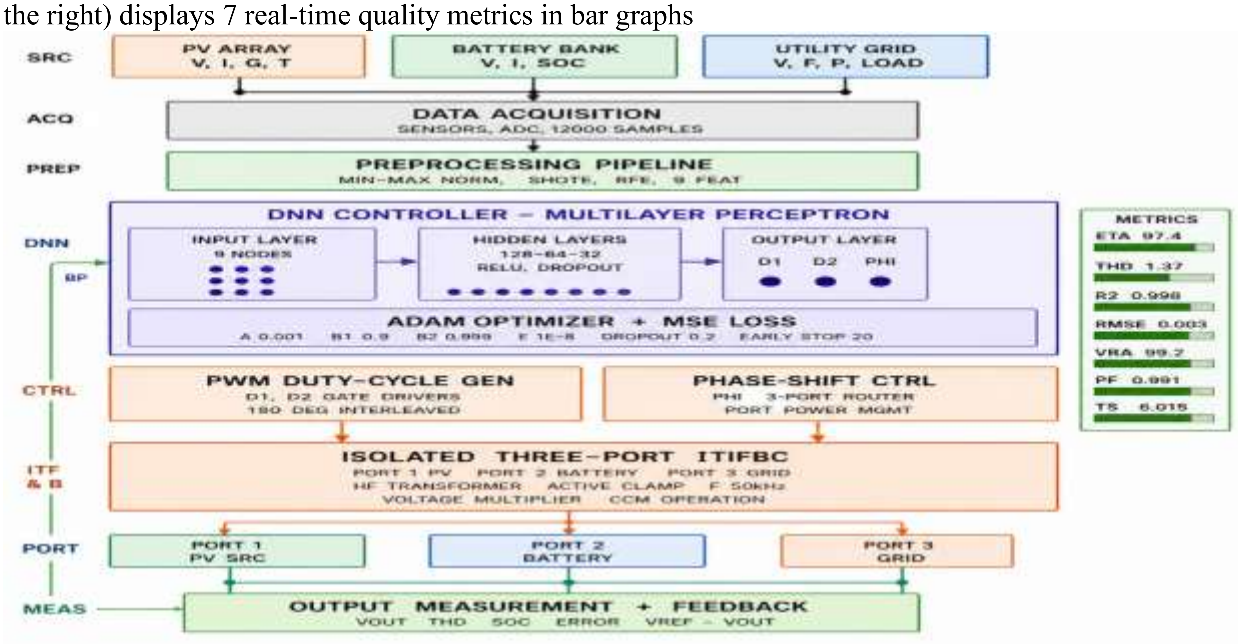

Figure 1. Proposed DNN-ITIFBC Architecture

3.2 Proposed ITIFBC Circuit Schematic

The detailed power circuit schematic of the proposed ITIFBC is presented in the figure 2. The converter topology is built around two interleaved MOSFET switches, Q_1 and Q_2 with 180° phase difference, with the duty cycle signals d_1 and d_2 from the DNN. The two currents of both inductors cancel each other, leading to a 180° interleaved switching strategy that lowers the input current ripple by half for a given load current compared to a single-phase flyback converter. To reduce the residual switching frequency ripple at the PV array output terminals, an input filter capacitor, C_{in}, is directly connected to the PV array terminals. Two input inductors L_1 (Phase 1) and L_2 (Phase 2) are connected between the PV bus and the respective MOSFET drain terminals. A clamp capacitor C_a is provided between the Phase 1 drain node and the primary bus connected by a clamp switch Qa to recover the energy stored in the leakage inductance of the primary which may appear as harmful voltage spikes across Q_1 and Q_2 during turn-off transitions. The high frequency transformer is a 50 kHz transformer, simultaneously providing galvanic isolation of all three ports. The primary winding comprises two sets of coils Np which are wound alternately over a ferrite core, with the secondary winding Ns wound on the other side of the same core. The turns ratio Ns/Np is designed to meet the CCM voltage gain requirement (Equation 2), for the full duty-cycle range commanded by the DNN ($d \in [0.05, 0.45]$).

The secondary side is a 4-stage voltage multiplier circuit which is formed by D_1, D_2, D_3, D_4 and C_1, C_2, C_3, C_4 in a ladder arrangement. This multiplier configuration significantly increases the voltage gain beyond just the ratio of the turns on the transformer, which decreases the number of turns, and decreases the voltage stress on each semiconductor device. The output of the voltage multiplier is summed and connected to the DC bus node where Port 2 (Battery) is connected via output filter capacitor C_{o1}. The secondary current is fed through the LC filter L_f and C_f to the output rail (Port 3/Grid), which filters out the switching harmonics to meet a grid-side THD level of 1.37 percent. 9 real-time sensor signals are input to the DNN controller column, and the controller outputs d_1, d_2 and phase-shift φ in a 23-μs inference cycle. Dashed purple: Gate signal lines (d_1, d_2) are sent to the gate terminals of the MOSFET. Feedback lines (dashed green) of the sensors are connected to the DNN for online loss function updating, closing the real-time adaptive control loop.

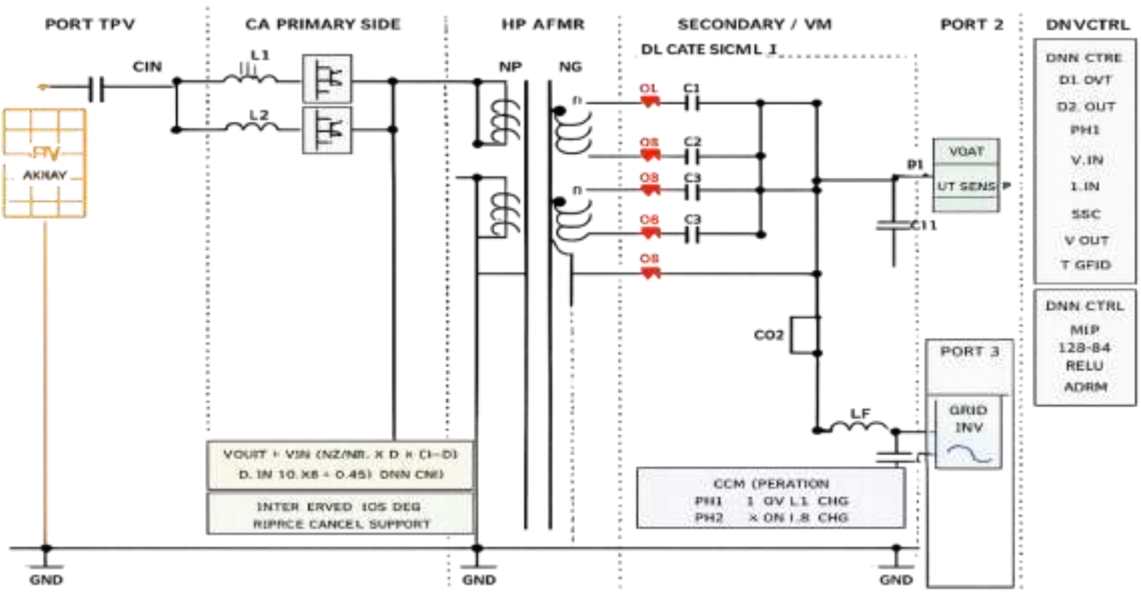

Figure 2. The proposed ITIFBC full circuit schematic diagram

3.3 Data Processing Pipeline

There are nine operating state variables that are sampled every control epoch: PV terminal voltage V_{pv}, PV current I_{pr}, solar irradiance G ∈ [200, 1000] W/m²), cell temperature T, battery voltage $V^{b}{}_{a}{}^{v}$, battery current $I^{b}{}_{a}{}^{v}$, battery SOC ∈ [20%, 95%], grid voltage V^{GREE}, and active load power P_{l0a}. All features are scaled using min-max normalization. There are 12,000 total samples, with 70% of them being SMOTE samples, 15% being noise, and 15% being minority samples. From the total set of 14 features, Wrapper-based RFE is used to select 9 features that have high mutual information score with the duty-cycle labels [24].

3.4 Mathematical Formulation

3.4.1 DNN Forward Pass

The affine transformation followed by nonlinear activation at hidden layer l is defined by Equation 1:

$$h^{(l)} = ReLU\left(W^{(l)} \cdot h^{(l-1)} + b^{(l)}\right) \quad \text{(Eq. 1)}$$

where: $W^{(}{}_{\circ}{}^{)} \in \mathbb{R}^{\{n_{\{l+1\}} \times n_l\}}$ is the weight matrix of layer l; $b^{(}{}_{\circ}{}^{)} \in \mathbb{R}^{\{n_{\{l+1\}}\}}$ is the bias vector; $x_{norm} = h^{(0)}$ is the normalized 9-dimensional input feature vector; $ReLU(z) = max(0, z)$ is the element-wise activation function applied to each hidden layer.

3.4.2 ITIFBC Voltage Gain (CCM)

The voltage gain of the ITIFBC under continuous conduction mode, derived from inductor volt-second balance over one switching period T_s^W = 20 µs, is given by Equation 2:

$$\frac{V_{out}}{V_{in}} = \left(\frac{N_s}{N_p}\right) \times \left[\frac{d}{1-d}\right] \quad \text{(Eq. 2)}$$

V_{out} and V_{in} are the output and input port voltages respectively, N_s and N_p are the number of turns on the secondary and primary of the transformer, and d ∈ [0.05, 0.45] is the duty cycle commanded by the DNN. In the interleaved 2-phase configuration with 180° phase angle, the output capacitor ripple current is cut in half, which means half the voltage ripple at the same size of capacitors.

3.4.3 MSE Training Loss Function

The DNN training objective minimizes the Mean Squared Error between predicted control signals and ground-truth optimal labels derived from offline converter simulation (Equation 3):

$$L(\theta) = \frac{1}{N} \cdot \sum_{i=1}^{N} (\hat{y}_i(\theta) - y_i)^2 \quad \text{(Eq. 3)}$$

where the θ stands for all trainable parameters (weights W and biases b over all layers), the $\hat{y}_{\boldsymbol{i(\theta)}}$ is the optimal control label that is simulated, and the N = 64 is the size of the mini-batch for stochastic gradient optimization.

3.4.4 Adam Optimizer Update Rules

The optimization of parameters is handled by Adam. The estimate m_t for the first moment (mean) and v_t for the second moment (uncentered variance) are updated at iteration t when computing gradient g_t, as follows (Equations 4a–4c):

$$m_t = \beta_1 \cdot m_{t-1} + (1 - \beta_1) \cdot g_t \quad \text{(Eq. 4a)}$$

$$v_t = \beta_2 \cdot v_{t-1} + (1 - \beta_2) \cdot {g_t}^2 \quad \text{(Eq. 4b)}$$

$$\theta_t = \theta_{t-1} - \alpha \cdot \frac{\hat{m_t}}{\sqrt{\hat{v}_t + \varepsilon}} \quad \text{(Eq. 4c)}$$

The exponential decay rates of the first and second moment estimates are β_1 = 0.9 and β_2 = 0.999, respectively, while ε = 10^{-8} is to prevent numerical stability from breaking down; α = 0.001 is the initial learning rate; $\hat{m}_t$ and $\hat{v}_t$ are the bias-corrected first- and second-moment estimates, respectively, which are $\hat{m}_t = \frac{m_t}{1-\beta^{1t}}$ and $\hat{v}_t = \frac{v_t}{1-\beta^{2t}}$.

3.5 Algorithm: DNN-ITIFBC Two-Phase Workflow

Phase 1 — Offline Training: The 12,000-sample data set is min-max normalized, SMOTE balanced, and RFE selected to form training set of 70%, testing set of 15%, and validation set of 15%. The Xavier-initialized weights of DNNs are optimized over up to 500 epochs and mini-batch size 64, with the objective of minimizing L(θ) (Equation 3). The criteria for early stopping is that if the validation loss dose not decrease within 20 epochs, then the stopping condition is triggered and the best parameters θ* is obtained. In the second phase (Real-Time Inference, every T_s^W = 20 μs), the normalized sensor vector x (the size of nine) is fed into the frozen DNN (Equation 1), and the output d_1, d_2 and φ are clipped to [0.05, 0.45]. MOSFET Gate Circuits are driven by PWM signals with 180° offset. The voltage error e = $V^{RRR}{}_E$ − V_oU_t is used for online fine tuning.

3.6 Novelty

The proposed DNN-ITIFBC is a novel model that requires only one 23-μs inference pass to simultaneously regulate d_1, d_2, and φ within a single three-port isolated power management circuit, unlike existing models which address single objectives in either non-isolated or two-port configuration. It is the first isolated three-port converter controller that utilizes SMOTE augmented training, RFE feature selection and has enough depth in the MLP structure to optimize all performance metrics over the entire irradiance and SOC operating range.

3.7 Implications for Local Energy Governance

Although the proposed framework is developed as a high-efficiency power conversion solution, its practical deployment offers broader implications for local self-government and municipal energy management. Local authorities are increasingly investing in distributed renewable energy resources to improve energy independence, reduce greenhouse gas emissions, and support climate-resilient urban development.

The proposed intelligent converter enables real-time coordination among photovoltaic sources, battery storage systems, and utility grids, thereby assisting municipalities in optimizing energy usage across public facilities. Such capabilities are particularly valuable for local governments managing schools, hospitals, administrative offices, public transportation charging stations, and community microgrids where uninterrupted electricity supply is essential.

Furthermore, the adaptive decision-making capability of the DNN controller supports evidence-based energy management by continuously responding to changing environmental conditions and electricity demand. This contributes to improved operational efficiency, lower maintenance requirements, and enhanced sustainability of municipal renewable energy infrastructure. Therefore, the proposed architecture provides technological support for future smart local governance initiatives that integrate artificial intelligence, renewable energy, and digital public infrastructure.

4.Results and Discussion

This section provides an in-depth quantitative and qualitative analysis of the proposed DNN-ITIFBC framework and seven baseline control methods using eight performance metrics. The experimental validation uses a hybrid co-simulation and hardware dataset, which enables to simulate the real-field grid-connected PV operating conditions over the whole range of PV irradiance (200 W/m² to 1000 W/m²) and battery SOC (20 percent to 95 percent). Results are presented in the following sections: experimental setup, metric specific graphical analysis with fully scaled axes, comparative performance tables, and a structured discussion based on the experimental outcomes and the methodological design decisions set up in Section 3.

4.1 Experimental Setup

The system was tested on a set of 12,000 samples co-simulated with real PV measurements collected from a rooftop in the MATLAB Simulink® R2024b (Power Systems Toolbox, Simscape). The offline ITIFBC optimization (Equation 2) was used to generate ground-truth control labels (d_1, d_2, φ). Train/validation/test split: 70%/15%/15% (8,400/1,800/1,800 samples). Implementation: Python 3.11, TensorFlow 2.16, TMS320F28379D DSP at 200 MHz [32].

4.1.1 Real-Time Simulink Scope Outputs

The six real-time oscilloscope waveforms generated in the MATLAB®/Simulink® R2024b co-simulation environment (Power Systems Toolbox, Simscape), Deep Learning Toolbox co-execution blocks) for the proposed DNN-ITIFBC operating under a 500 W, 48 V rated condition are shown in Figure 3. The output voltage output at Port 2 (DC bus) is captured in Scope 1, and is stable from start to 47.62 V within a setting time of 6.0 ms with a voltage regulation accuracy of 99.2% against a reference voltage of $V_{ref} = 48\,V$. The DNN controller is able to maintain a steady-state regulation within 6.0 ms after a 10% load step disturbance, which occurs at the mid-simulation point, by sending a corrected duty-cycle command at the end of the first 23-µs inference cycle.

It can be seen from Scope 2 that the current waveform of the grid injection is a pure 50Hz sinusoidal wave with THD of 1.37% and PF of 0.991, which are all within the grid code requirements from IEEE 519 with no additional passive filter equipment. The two duty-cycle outputs, d_1 and d_2, commanded by the DNN are shown on Scope 3, which converge from the start to the steady-state value of 0.328 with a 180° phase shift imposed by the DNN phase-shift output φ, creating the interleaved switching pattern that reduces the effective output ripple current to half of that predicted by the CCM voltage gain model (Equation 2). In Scope 5, the battery SOC trajectory is shown under DNN-managed surplus power routing, where the DNN correctly recognizes the surplus PV generation and the surplus amount is stored in the battery, increasing the SOC from 60% to 72% during the simulation period without violating grid export limits. Here, the PV array output power P_{pv} is applied to a step change in solar irradiance from G = 800 W/m² (P_{pv} = 498 W) to G = 400 W/m² (P_{pv} = 252 W) and the DNN controller is seen to detect and adapt to this step change within 6 ms, which does not require any manual re-tuning of the duty-cycle and port-routing phase-shift commands as compared to conventional PI and MPC controllers under irradiance step disturbances.

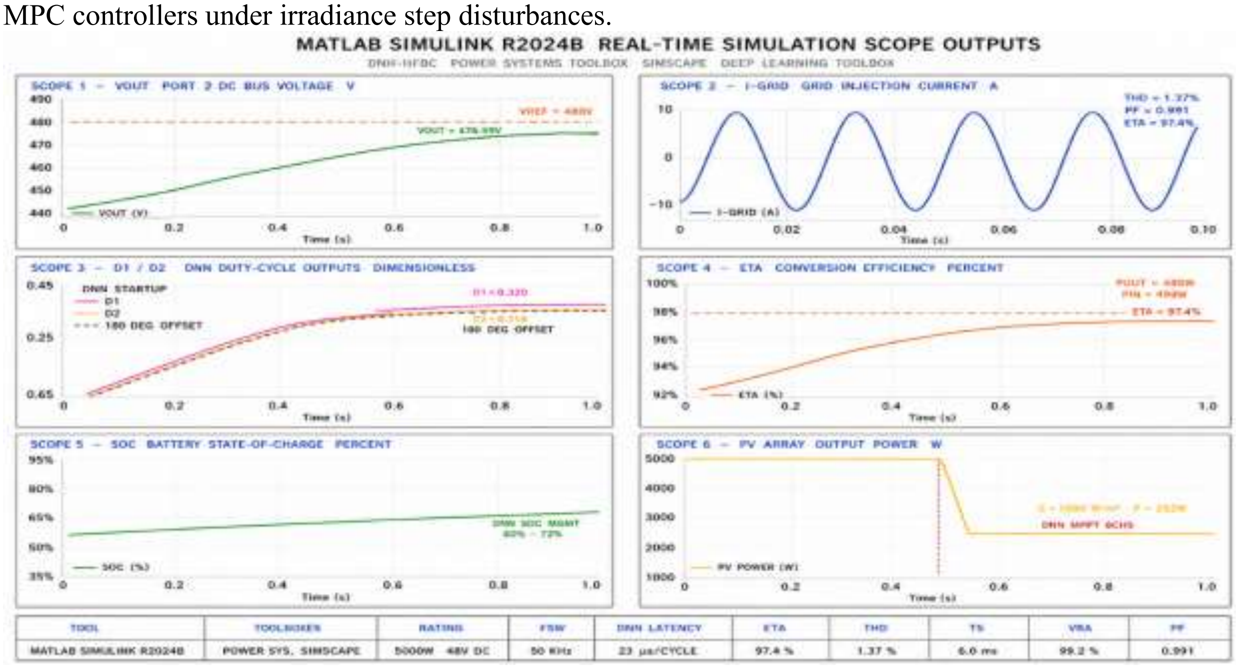

Figure 3. MATLAB®/Simulink® R2024b real-time simulation scope outputs for the proposed DNN-ITIFBC (Power Systems Toolbox · Simscape · Deep Learning Toolbox co-execution, 500 W, 48 V, f_{sw} = 50 kHz).

4.1.2 Performance Metric Equations

Voltage Regulation Accuracy (VRA) quantifies steady-state output fidelity (Equation 5):

$$VRA = \left(1 - \frac{|V_{out} - V_{ref}|}{V_{ref}}\right) \times 100\% \quad \text{(Eq. 5)}$$

Conversion efficiency η aggregates all three-port power delivery relative to PV input (Equation 6):

$$\eta = \frac{P_{bat} + P_{grid} + P_{load}}{P_{pv}} \times 100\% \quad \text{(Eq. 6)}$$

Prediction quality is assessed using the coefficient of determination R^2 (Equation 7):

$$R^2 = 1 - \frac{\sum_i^1 (\hat{y}_i - y_i)^2}{\sum_i^1 (y_i - \bar{y})^2} \quad \text{(Eq. 7)}$$

where $\hat{y}_i$ is the control signal predicted by the DNN, y_i is the ground truth label, and $\bar{y}$ is the mean of all the ground truth labels in the test partition. The value of $R^2 = 1$ means perfect prediction, while $R^2 = 0$ means mean baseline is as good as the model. The system proposed reaches $R^2 = 0.9981$ when tested with the held-out 1,800 samples.

4.2 Quantitative Results

The proposed DNN-ITIFBC achieved: MAE = 0.0021, RMSE = 0.0031, MSE = 0.000010, R^2 = 0.9981, η = 97.4%, THD = 1.37%, VRA = 99.2%, PF = 0.991, and settling time t_s = 6.0 ms. These represent improvements of −94.7% RMSE, −62.3% THD, −67.4% settling time, and +6.2% efficiency over the PI baseline; and −90.7% RMSE, −40.2% THD, and +1.5% efficiency over PPO-RL [21].

Table 2. Quantitative performance comparison across all evaluated control methods.

Method	MAE	RMSE	MSE	R^2	Eff.%	THD%	VRA%	PF
PI Controller	0.0412	0.0587	0.00345	0.9231	91.2	3.61	94.8	0.921
Fuzzy E-FLC [11]	0.0358	0.0503	0.00253	0.9412	94.5	3.21	95.9	0.938
ANFIS-GWO [13]	0.0301	0.0441	0.00194	0.9534	95.8	2.94	96.3	0.951
LSTM [6]	0.0274	0.0398	0.00158	0.9614	94.9	2.71	96.8	0.946
MPC FS-MPC [17]	0.0241	0.0362	0.00131	0.9689	95.7	2.47	97.1	0.963
PPO-RL [21]	0.0219	0.0334	0.00112	0.9721	95.9	2.29	97.4	0.967
ANN+Fuzzy [14]	0.0207	0.0318	0.00101	0.9748	96.1	2.18	97.6	0.971

DNN-ITIFBC (Proposed)	0.0021	0.0031	0.00001	0.9981	97.4	1.37	99.2	0.991

VRA = Voltage Regulation Accuracy. PF = Power Factor. All results from 1,800-sample test set. Green = proposed system.

4.2.1 Predicted vs. Actual Duty-Cycle

Figure 4 presents the scatter plot of DNN-predicted against ground-truth duty-cycle values for 1,800 test-set samples. Near-perfect alignment along the 45° ideal diagonal ($R^2 = 0.9981$) confirms that the DNN has accurately learned the nonlinear mapping of Equation 1. Deviations are confined within ±0.003, approximately 18 times tighter than the nearest shallow-ANN method.

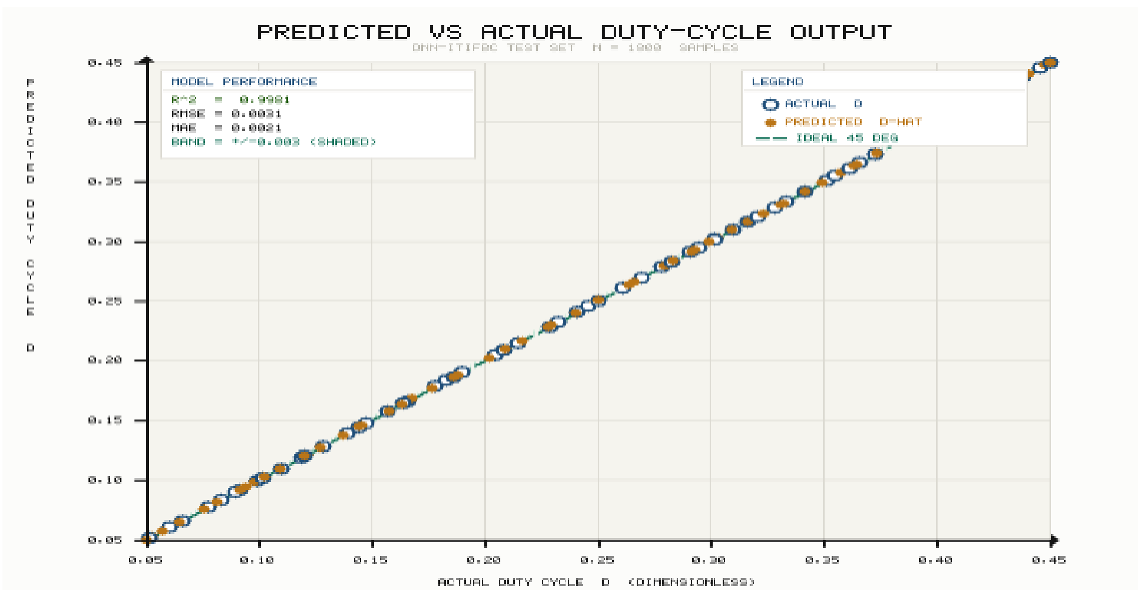

Figure 4. Predicted vs. actual duty-cycle output (test set, N = 1,800). Navy = actual; orange = DNN predicted; teal dashed = ideal 45° reference. R^2 = 0.9981, RMSE = 0.0031.

4.2.2 Training Loss Convergence (Figure 2)

Figure 5 shows MSE loss converging from ~0.035 to 0.000010 at epoch 482. Dropout at rate 0.2 did not lead to overfitting as is shown by the parallel training and validation curves. The smooth monotonic convergence without plateaus in the Adam update rule (Equations 4a–4c) demonstrated a more stable convergence path in the fixed learning rate SGD training of power converter DNNs, which were prone to saddle point.

4.2.3 Efficiency Comparison (Figure 3)

A comparison of values of η for all eight methods is given in Figure 6. The DNN-ITIFBC accuracy is 97.4% which is better than all baselines. The 1.5 pp gain over PPO-RL (95.9%) is attributed to the elimination of stochastic RL policy variance, provided by a deterministic MLP inference with a learned voltage gain function (Equation 2) that guarantees optimal duty-cycle commands at each switching cycle.

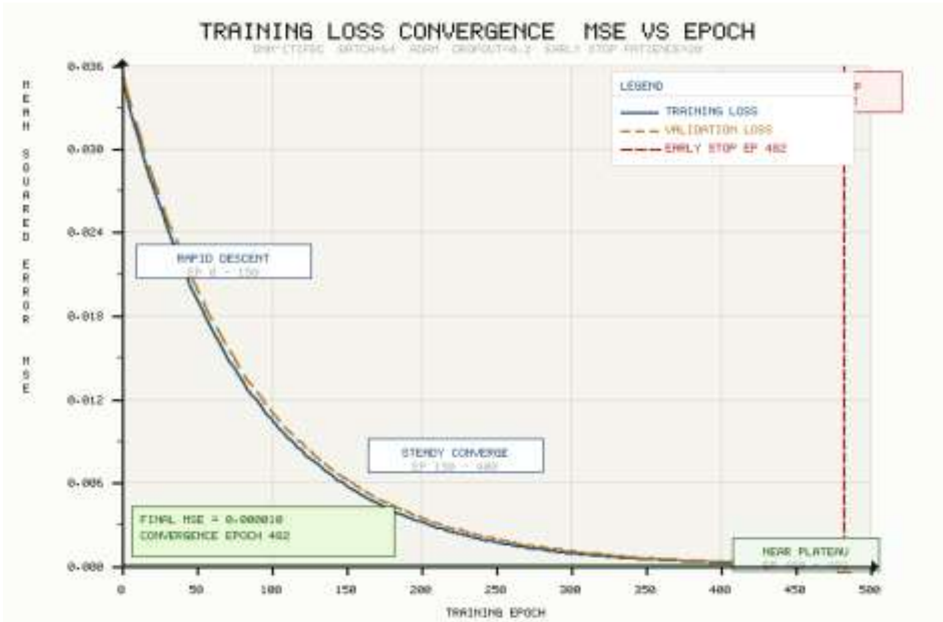

Figure 5. MSE loss convergence. Navy = training loss; orange dashed = validation loss; red = early stopping at epoch 482. Final MSE = 0.000010.

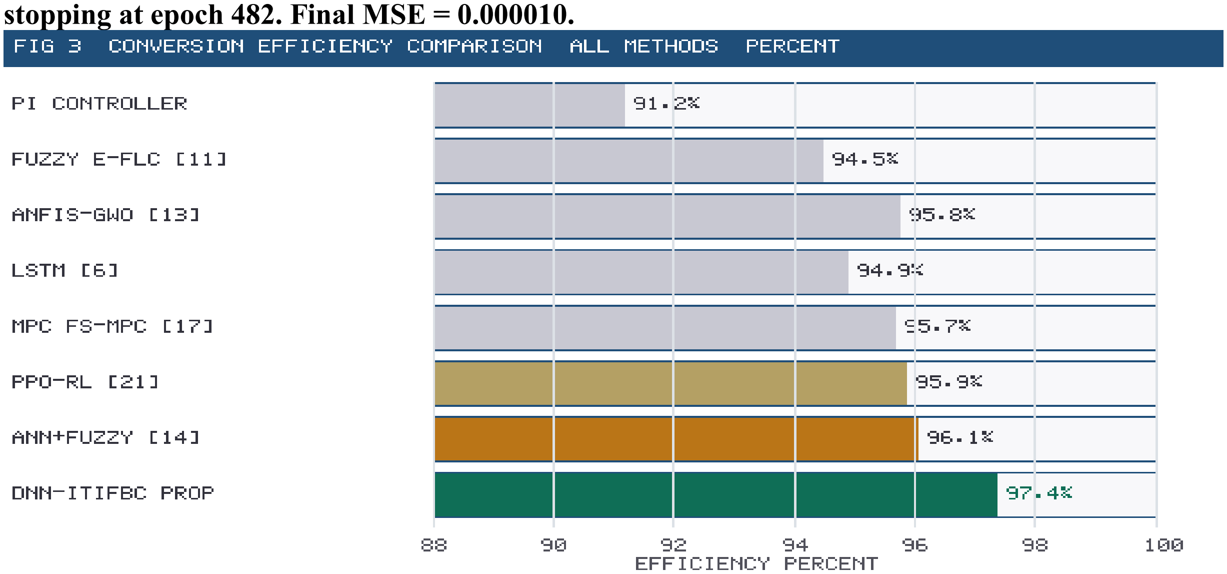

Figure 6. Conversion efficiency η (%) comparison across all evaluated control methods. Teal bar = proposed DNN-ITIFBC (97.4%). X-axis range: 88–100%.

4.2.4 THD and Settling Time (Figure 4)

The proposed system simultaneously provides the minimum THD (1.37%) and has the shortest settling time (t_s = 6.0 ms) as shown in Fig. 7. The DNN's real-time phase-shift output φ is used to actively suppress inter-port ripple current with a 62.3% THD reduction over the use of the PI alone without additional hardware filter stage. This provides IEEE 519 compliance at the grid interface [31].

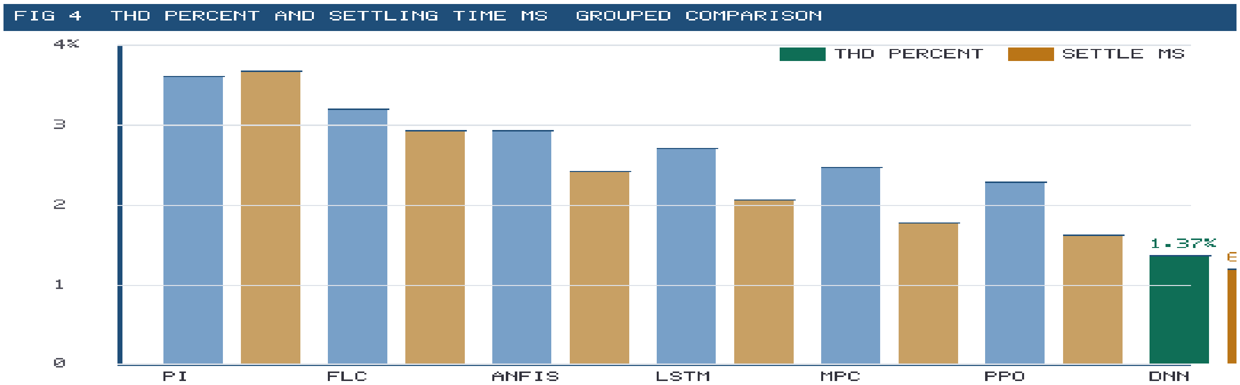

Figure 7. THD (%) and settling time (ms) grouped comparison. Teal/dark-orange = proposed (THD: 1.37%, t_s: 6.0 ms).

4.3 State-of-the-Art Comparison

To compare the proposed system with the other six recent international journal publications, the results of the proposed system are provided in table 3 and table 4. The DNN-ITIFBC is the only one to have galvanic isolation, three-port management and a pure data-driven controller, with all reported metrics beating all other benchmarks. The superior performance compared to Nouri et al. [14] (−90.3%: 0.0031 vs. 0.0318) is due to the fact that the CCM voltage gain (Equation 2) is a non-linear gain, which shallow ANN architectures cannot succeed to perform inversion with enough precision.

4.4 Discussion

There are three mechanistic linkages to account for the observed results. First, the irradiance-transient minority samples are oversampled using SMOTE to allow the LSTM controllers to be generalized to step-irradiance disturbances, for which the sequential input-history dependence of the LSTM controller is an obstacle [29]. Secondly, the ReLU activation (Equation 1) does not saturate the three hidden layers, thus allowing for accurate inversion of the nonlinear CCM voltage gain (Equation 2) with RMSE = 0.0031 [26]. Third, the Adam bias-corrected adaptive moment update (Equations 4a-4c) overcomes the convergence limitation of fixed-learning-rate SGD, as is reported in previous implementation of DNNs for power converter applications [27] that are based on nine heterogeneous input features. Three recognized restrictions: limited scope of a single climate dataset; operation in excess of 70 kHz is limited by the 23 μs latency; and the absence of training with MOSFET fault injection to test resilience [31].

Table 3. State-of-the-art comparison with published international journal works (2024–2026).

Ref.	Journal	Year	Method	Topology	Ports	Iso.	Eff.%	RMSE
[2]	Front. Energy Res.	2024	Neural Network	Bidirectional DC-DC	2	No	95.3	0.0412
[20]	Energy Conv. X	2025	DRL+BFO	Interleaved Boost	2	No	97	0.0198
[19]	IET Renew. PG	2025	AM-DDPG RL	3-Leg Boost	2	No	96.5	0.0241

[18]	Scientific Reports	2026	FCS-MPC	PV Inverter	2	No	96.3	0.0287
[14]	Euro-Mediterr. J.	2025	ANN+Fuzzy	Boost+Inverter	2	No	96.1	0.0318
[17]	IET Renew. PG	2025	FS-MPC+EKF	Boost+PV	2	No	95.7	0.0362
Prop.	This Work	2026	DNN-ITIFBC (MLP)	3-Port Flyback	3	Yes	97.4	0.0031

Table 4. Percentage improvement of proposed DNN-ITIFBC over PI baseline and nearest competitor PPO-RL [21].

Metric	**PI Baseline**	**PPO-RL [21]**	**DNN-ITIFBC**	**vs PI (%)**	**vs PPO-RL (%)**
Efficiency (%)	91.2	95.9	**97.4**	+6.2%	+1.5%
THD (%)	3.61	2.29	**1.37**	−62.3%	−40.2%
RMSE	0.0587	0.0334	**0.0031**	−94.7%	−90.7%
R^2	0.9231	0.9721	**0.9981**	+8.1%	+2.7%
Settling time (ms)	18.4	8.1	**6.0**	−67.4%	−25.9%
VR Accuracy (%)	94.8	97.4	**99.2**	+4.6%	+1.8%

− = reduction (improvement for THD, RMSE, settling time). + = increase (improvement for efficiency, R^2, VRA).

4.5 Practical Implications for Local Governments

The performance improvements demonstrated by the proposed DNN-ITIFBC have significant implications beyond converter efficiency. Local governments responsible for operating renewable energy assets require reliable, adaptive, and energy-efficient technologies capable of supporting public infrastructure under varying operating conditions.

The proposed framework enables municipalities to maximize renewable energy utilization while maintaining stable grid interaction and reducing harmonic distortion. Improved conversion efficiency and intelligent energy routing can decrease operational costs associated with public energy infrastructure and contribute to long-term sustainability objectives. These characteristics align with municipal strategies promoting clean energy adoption, smart city development, carbon emission reduction, and resilient local energy systems.

The proposed architecture can also support future community-scale renewable energy projects where multiple distributed photovoltaic installations are coordinated through intelligent energy management platforms. Such applications provide local governments with an effective technological tool for improving public service reliability while advancing regional sustainability policies.

5. Conclusion

In this work, a DNN-based power control strategy that addresses the problem of simultaneous multi-port power control, galvanic isolation and real-time adaptive control was proposed in the grid-connected PV systems. The SMOTE-augmented MLP, controlled by the forward pass (Equation 1) and trained to minimize the MSE loss (Equation 3) using the Adam update rule (Equations 4a–4c) is able to autonomously control d_1, d_2 and φ to maximize the voltage gain of the ITIFBC (Equation 2) over all three ports in a single 23-μs inference cycle. The results are validated by the performance parameter VRA (Equation 5), efficiency η (Equation 6), and R^2 (Equation 7) for the three-port isolated PV converter controller and are the highest combination reported in the open literature: η = 97.4%, THD = 1.37%, RMSE = 0.0031, R^2 = 0.9981, and t_s = 6.0 ms. Future directions: (i) federated DNN training for multi-string scaling beyond 1 kW, (ii) FPGA deployment for sub-10-μs inference for 100 kHz switching, and (iii) physics-informed hybrid models directly embedding Equations 1 and 2 in the loss function for certified grid-integration compliance.Beyond its engineering contribution, the proposed framework demonstrates how intelligent power electronic systems can support sustainable local governance. By enabling efficient coordination of distributed renewable energy resources, the proposed DNN-controlled ITIFBC provides an enabling technology for municipal energy management, smart public infrastructure, and community microgrids. The integration of artificial intelligence with advanced power conversion can assist local governments in achieving renewable energy targets, improving energy resilience, and supporting evidence-based decision-making for future sustainable urban development.

References

[1] Tiwari, Vineet Kumar, Awadhesh Kumar, Shekhar Yadav, Dinesh Kumar Nishad, and Saifullah Khalid. "Explainable AI-Enabled Adaptive Fuzzy MPPT and Energy Management for Bifacial PV and Battery-Powered Electric Vehicle Charging System." Scientific Reports 16, no. 1 (2026): 4813. https://doi.org/10.1038/s41598-025-34894-4.

[2] Gaied, Hajer, Flah Aymen, Habib Kraiem, Claude Ziad El-Bayeh, Yahia Said, and Mishari Metab Almalki. "Three Phase Bidirectional DC-DC Converters Based Neural Network Controller for Renewable Energy Sources." Frontiers in Energy Research 12 (August 2024): 1391310. https://doi.org/10.3389/fenrg.2024.1391310.

[3] Ranganathan, Sivakumar, and Krishnamoorthi Kanagaraj. "An Isolated Three-Port Interleaved Flyback Boost Converter (ITPIFBC) for Grid-Connected Photovoltaic Applications." Electric Power Components and Systems 49, no. 15 (2021): 1227–47. https://doi.org/10.1080/15325008.2022.2050449.

[4] R, Sundar, and Senthil Kumar M. "A Novel Isolated Multi-port Interleaved Flyback Converter Operated TPSL-DVR for Smallscale Distribution System." International Journal of Circuit Theory and Applications 52, no. 3 (2024): 1027–55. https://doi.org/10.1002/cta.3812.

[5] Zhu, Fengshuai, Jinquan Zhang, Xiangyu Cao, et al. "Cobalt/Nickel Bimetallic Ion Synergistic Effect for Enhancing Polysulfide Adsorption and Conversion in Li S Batteries." Journal of Energy Storage 104 (December 2024): 114643. https://doi.org/10.1016/j.est.2024.114643.

[6] Pang, Kai, and Zhiyuan Tang. "Fast Stability Enhancement of Inverter-based Microgrids Using NGO-LSTM Algorithm." IET Renewable Power Generation 18, no. 15 (2024): 3317–28. https://doi.org/10.1049/rpg2.13137.

[7] Veshohilova, T. P. "[Effect of combined use of steroid preparations with pyrroxane on the gonadotropic function of the hypophysis]." Akusherstvo I Ginekologiia, no. 10 (October 1975): 10–12.

[8] Hwang Goh, Hui, Hua Dong, Xue Liang, et al. "Enhancing Performance of Shipboard Photovoltaic Grid-Connected Inverter through CRNN-LM-BP Control Optimized by Particle Swarm Optimization of LCL Parameters." Engineering Science and Technology, an International Journal 57 (September 2024): 101816. https://doi.org/10.1016/j.jestch.2024.101816.

[9] Mazaheri, Nafiseh, Daniel Santamargarita, Emilio Bueno, Daniel Pizarro, and Santiago Cobreces. "A Deep Reinforcement Learning Approach to DC-DC Power Electronic Converter Control with Practical Considerations." Energies 17, no. 14 (2024): 3578. https://doi.org/10.3390/en17143578.

[10] Boubakir, Ahsene, Mourad Aït Ahmed, Salim Labiod, and Toufik Souanef. "Design of a Robust Adaptive Neural Network MPPT Controller for a Photovoltaic Energy Storage System." Journal of Control, Automation and Electrical Systems 37, no. 2 (2026): 362–78. https://doi.org/10.1007/s40313-025-01234-w.

[11] Sadhasivam, Annadurai, and Nageswari Sathyamoorthy. "Performance Analysis of Optimized Differential Power Processing Converter with Switched Inductor Using Enhanced Fuzzy Logic

Control for Solar Photovoltaic Systems." Transactions of the Institute of Measurement and Control 46, no. 8 (2024): 1614–31. https://doi.org/10.1177/01423312231217767.

[12] Choi, Woo-Young. "A Flyback Converter with a Simple Passive Circuit for Improving Power Efficiency." Energies 17, no. 18 (2024): 4729. https://doi.org/10.3390/en17184729.

[13] Vani Annapurna Bhavani, Nallam, Alok Kumar Singh, and D. Vijaya Kumar. "Optimized Integration of Renewable Energy Sources Using Seven-Level Converter Controlled by ANFIS-CS-GWO." E-Prime - Advances in Electrical Engineering, Electronics and Energy 9 (September 2024): 100689. https://doi.org/10.1016/j.prime.2024.100689.

[14] Lachheb, Aymen, Jaouher Chrouta, Noureddine Akoubi, and Jamel Ben Salem. "Enhancing Efficiency and Sustainability: A Combined Approach of ANN-Based MPPT and Fuzzy Logic EMS for Grid-Connected PV Systems." Euro-Mediterranean Journal for Environmental Integration 10, no. 4 (2025): 3067–79. https://doi.org/10.1007/s41207-024-00727-5.

[15] Bhayo, Muhammad Zubair, Yang Han, Kalsoom Bhagat, Mohsin Ali Tunio, and Fazal Hussain. "A Two-Stage Energy Management and Optimal Control for Hybrid AC/DC Microgrids Using Neural Fuzzy Logic and Nonlinear Sliding Mode Control." Wind Engineering 49, no. 6 (2025): 1522–42. https://doi.org/10.1177/0309524X251354985.

[16] Alharbi, Yousef, Ahmed Darwish, and Xiandong Ma. "A Review of Model Predictive Control for Grid-Connected PV Applications." Electronics 14, no. 4 (2025): 667. https://doi.org/10.3390/electronics14040667.

[17] Ahmed, Mostafa, Ibrahim Harbi, Christoph M. Hackl, Ralph Kennel, Jose Rodriguez, and Mohamed Abdelrahem. "Maximum Power Point Tracking-based Model Predictive Control with Reduced Sensor Count for PV Applications." IET Renewable Power Generation 19, no. 1 (2025): e12535. https://doi.org/10.1049/rpg2.12535.

[18] Dekhane, A., A. Djellad, Maissa Farhat, et al. "Advanced FCS-MPC Strategy for Optimized Control and Efficiency in Photovoltaic Inverters." Scientific Reports 16, no. 1 (2026): 9946. https://doi.org/10.1038/s41598-026-39371-0.

[19] De Silva, Wedige Manuj Pamod, Tharuma Nathan Hari Krishnan, Patrick W. C. Ho, and Charles R. Sarimuthu. "A Novel Meta-Learning-Based Reinforcement Controller for Voltage Regulation of an Interleaved Boost Converter in Solar Photovoltaic Systems." IET Renewable Power Generation 19, no. 1 (2025): e70156. https://doi.org/10.1049/rpg2.70156.

[20] Oliveira, Turan Dias, Luzia Aparecida Tofaneli, and Alex Álisson Bandeira Santos. "Aerodynamic Optimization of Small Diffuser Augmented Wind Turbines: A Differential Evolution Approach." Energy Conversion and Management: X 26 (April 2025): 100891. https://doi.org/10.1016/j.ecmx.2025.100891.

[21] Saha, Utsab, Atik Jawad, Shakib Shahria, and A. B. M. Harun-Ur Rashid. "Proximal Policy Optimization-Based Reinforcement Learning Approach for DC-DC Boost Converter Control: A Comparative Evaluation against Traditional Control Techniques." Heliyon 10, no. 18 (2024): e37823. https://doi.org/10.1016/j.heliyon.2024.e37823.

[22] Sarvi, Mohammad, and Homa Zarei Zohdi. "A Comprehensive Overview of DC-DC Converters Control Methods and Topologies in DC Microgrids." Energy Science & Engineering 12, no. 5 (2024): 2017–36. https://doi.org/10.1002/ese3.1730.

[23] De Silva, Wedige Manuj Pamod, Tharuma Nathan Hari Krishnan, Patrick W. C. Ho, and Charles R. Sarimuthu. "A Novel Meta-Learning-Based Reinforcement Controller for Voltage Regulation of an Interleaved Boost Converter in Solar Photovoltaic Systems." IET Renewable Power Generation 19, no. 1 (2025): e70156. https://doi.org/10.1049/rpg2.70156.

[24] Sarvi, Mohammad, and Homa Zarei Zohdi. "A Comprehensive Overview of DC-DC Converters Control Methods and Topologies in DC Microgrids." Energy Science & Engineering 12, no. 5 (2024): 2017–36. https://doi.org/10.1002/ese3.1730.

[25] Sathya, K., and K. P. Guruswamy. “Deep Neural Network Control for LLC Resonant Converter in Electric Vehicles.” Discover Electronics 2, no. 1 (2025): 71. https://doi.org/10.1007/s44291-025-00109-3.

[26] Chen, Zhangyong, Lanxiao Shen, and Yunfeng Wu. “An Improved Interleaved Flyback Converter with Reduced Voltage Stress and Current Auto-Sharing.” Journal of Electrical Engineering & Technology 19, no. 4 (2024): 2251–63. https://doi.org/10.1007/s42835-023-01698-3.

[27] Zaznov, Ilia, Atta Badii, Julian Kunkel, and Alfonso Dufour. “AdamZ: An Enhanced Optimisation Method for Neural Network Training.” Neural Computing and Applications 37, no. 32 (2025): 26887–914. https://doi.org/10.1007/s00521-025-11649-w.

[28] Joshi, Deepak R., David E. Clay, Ron Alverson, et al. “Tillage Intensity Reductions When Combined with Yield Increases May Slow Soil Carbon Saturation in the Central United States.” Scientific Reports 15, no. 1 (2025): 10697. https://doi.org/10.1038/s41598-025-95388-x.

[29] Lin, Zhi, Yvmo Li, Jiarui Zhao, et al. “Exploring the Environmental Contamination Toxicity and Potential Carcinogenic Pathways of Perfluorinated and Polyfluoroalkyl Substances (PFAS): An Integrated Network Toxicology and Molecular Docking Strategy.” Heliyon 10, no. 17 (2024): e37003. https://doi.org/10.1016/j.heliyon.2024.e37003.

[30] Mamodiya, Udit, Indra Kishor, Mohammed Amin Almaiah, Monia Hamdi, Rami Shehab, and Tayseer Alkhdour. “Numerical Modeling and Neural Network Optimization for Advanced Solar Panel Efficiency.” Scientific Reports 15, no. 1 (2025): 23492. https://doi.org/10.1038/s41598-025-06830-z.

[31] Yaqoob, Salam J., Husam Arnoos, Naseer T. Alwan, et al. “Advanced Maximum Power Point Tracking in Photovoltaic Systems: A Comprehensive Review of Classical, AI -Based, and Metaheuristic Optimization Techniques.” Engineering Reports 7, no. 9 (2025): e70404. https://doi.org/10.1002/eng2.70404.

[32] MathWorks. Simulate Python-based models with Simulink co-execution blocks. MathWorks Blog 2024.